Volume 6 | Number 28 | 28 July 2018 | Pages 7405–7702

# Journal of Materials Chemistry C

Materials for optical, magnetic and electronic devices

rsc.li/materials-c

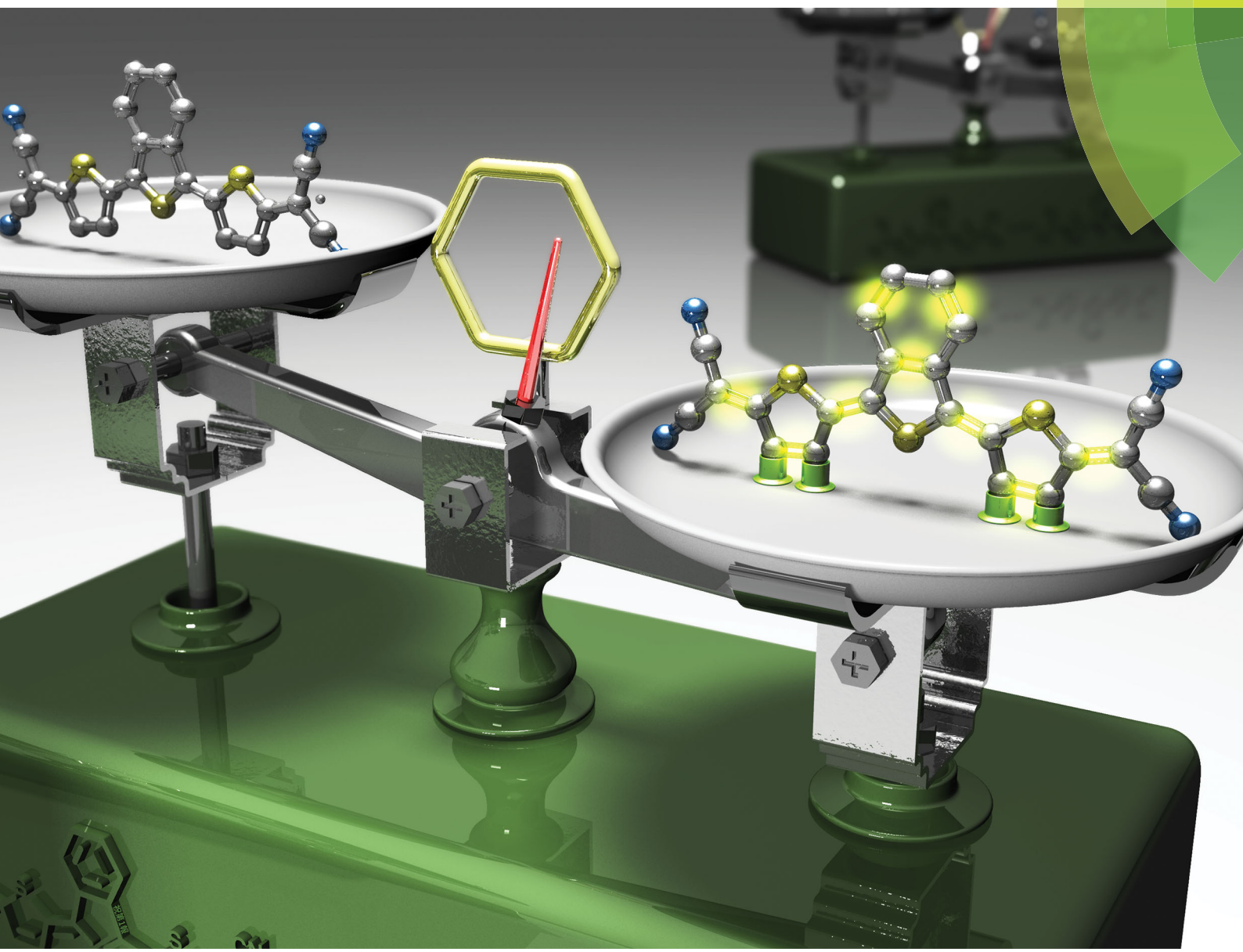

ISSN 2050-7526

ROYAL SOCIETY OF CHEMISTRY

PAPER

Yutaka Ie, Yoshio Aso *et al.*

Oligothiophene quinoids containing a benzo[*c*]thiophene unit for the stabilization of the quinoidal electronic structure

Journal of Materials Chemistry C

PAPER

View Article Online
View Journal | View Issue



Cite this: J. Mater. Chem. C, 2018, 6, 7493

# Oligothiophene quinoids containing a benzo[c]thiophene unit for the stabilization of the quinoidal electronic structure†

Keitaro Yamamoto,[a] Yutaka Ie,*[abc] Masashi Nitani,[a] Norimitsu Tohnai,[d] Fumitoshi Kakiuchi,[be] Ke Zhang,[c] Wojciech Pisula,[cf] Kamal Asadi,[c] Paul W. M. Blom[c] and Yoshio Aso*[a]

Received 17th April 2018,
Accepted 17th May 2018

DOI: 10.1039/c8tc01802b

rsc.li/materials-c

Bis(dicyanomethylene)-substituted quinoidal π-conjugated systems possess a high electron-accepting nature and thus have been extensively investigated for application as n-type semiconductors. We focus on the utilization of benzene-annelation for the stabilization of the quinoidal electronic structure against the biradicaloid structure by designing quinoidal thiophenes 3-mer (**BTQ**) and 6-mer (**BTQ-6**) that have benzo[*c*]thiophene units. We also develop quinoidal oligothiophenes (**BTQ-F**) consisting of both benzo[*c*]thiophene and fluorinated thiophene units. The influence of benzo[*c*]thiophene on the quinoidal electronic structure is investigated by theoretical studies and property measurements. The molecular structure of **BTQ-F** is unambiguously confirmed through single-crystal X-ray diffraction. Analyses of cyclic voltammetry reveal that the lowest unoccupied molecular orbital energy levels of these compounds lie below −4.0 eV, leading to good electron-transporting characteristics even under ambient conditions in organic field-effect transistors (OFETs). Due to an increased highest occupied molecular orbital energy level, ambipolar transport is observed in **BTQ-6**, indicating the versatility of quinoidal π-conjugated systems incorporating benzo[*c*]thiophene.



## Introduction

Significant research interest continues to be focussed on structurally well-defined π-conjugated oligomers, not only for the elucidation of fundamental structure–property relationship, but also for their applications in organic thin-film electronics such as organic field-effect transistors (OFETs) and organic photovoltaics.[1,2] π-Conjugated compounds bearing quinoidal structures have been extensively investigated not only as a model structure of doped conducting arylene polymers, but also as a Wurster-type multi-redox system in Hünig's classification.[3] Among them, bis(dicyanomethylene)-substituted quinoidal compounds, which generate an anionic aromatic state by accepting one or two electrons, exhibit a high electron-accepting ability for instance the well-known compound tetracyano-*p*-quinodimethane.[4] Therefore, the extension of the π-conjugation of such quinoidal systems, typically tetracyano quinoidal oligothiophenes, has attracted great attention for promising electron-transporting (n-type) semiconductors.[5–13] Another unique feature of the quinoidal systems is the equilibrium between quinoidal and biradicaloid electronic structures,[14] which causes a configurational instability of quinoidal oligothiophenes. A representative approach to increase the contribution of the quinoid character in oligothiophenes involves the utilization of aromatic stabilization in the quinoidal form, which was accomplished by the introduction of a fused aromatic ring on the thiophene [*c*]bond, as observed first in the synthesis of poly(isothianaphthene) with a small band gap by Wudl *et al.*[15] In this context, quinoidal oligothiophenes containing thieno[3,4-*b*]thiophene have been extensively developed by Zhu *et al.*[16] We envisioned that if the benzo[*c*]thiophene (isothianaphthene) quinoid unit can be incorporated into π-extended quinoidal structures, the high aromatic stabilization energy of this unit

[a] The Institute of Scientific and Industrial Research (ISIR), Osaka University, 8-1 Mihogaoka, Ibaraki, Osaka 567-0047, Japan. E-mail: yutakaie@sanken.osaka-u.ac.jp, aso@sanken.osaka-u.ac.jp
[b] Japan Science and Technology (JST) Agency, ACT-C, 4-1-8 Honcho, Kawaguchi, Saitama, 332-0012, Japan
[c] Max Planck Institute for Polymer Research, Ackermannweg 10, Mainz 55128, Germany
[d] Department of Materials and Life Science, Graduate School of Engineering, Osaka University, 2-1 Yamadaoka, Suita, Osaka 565-0871, Japan
[e] Department of Chemistry, Faculty of Science and Technology, Keio University, 3-14-1 Hiyoshi, Kohoku-ku, Yokohama, Kanagawa 223-8522, Japan
[f] Department of Molecular Physics, Faculty of Chemistry, Lodz University of Technology, Zeromskiego 116, Lodz 90-924, Poland

† Electronic supplementary information (ESI) available: The results of synthetic details, NMR measurements, X-ray information, OFET device information, and computational details. CCDC 1837054. For ESI and crystallographic data in CIF or other electronic format see DOI: 10.1039/c8tc01802b

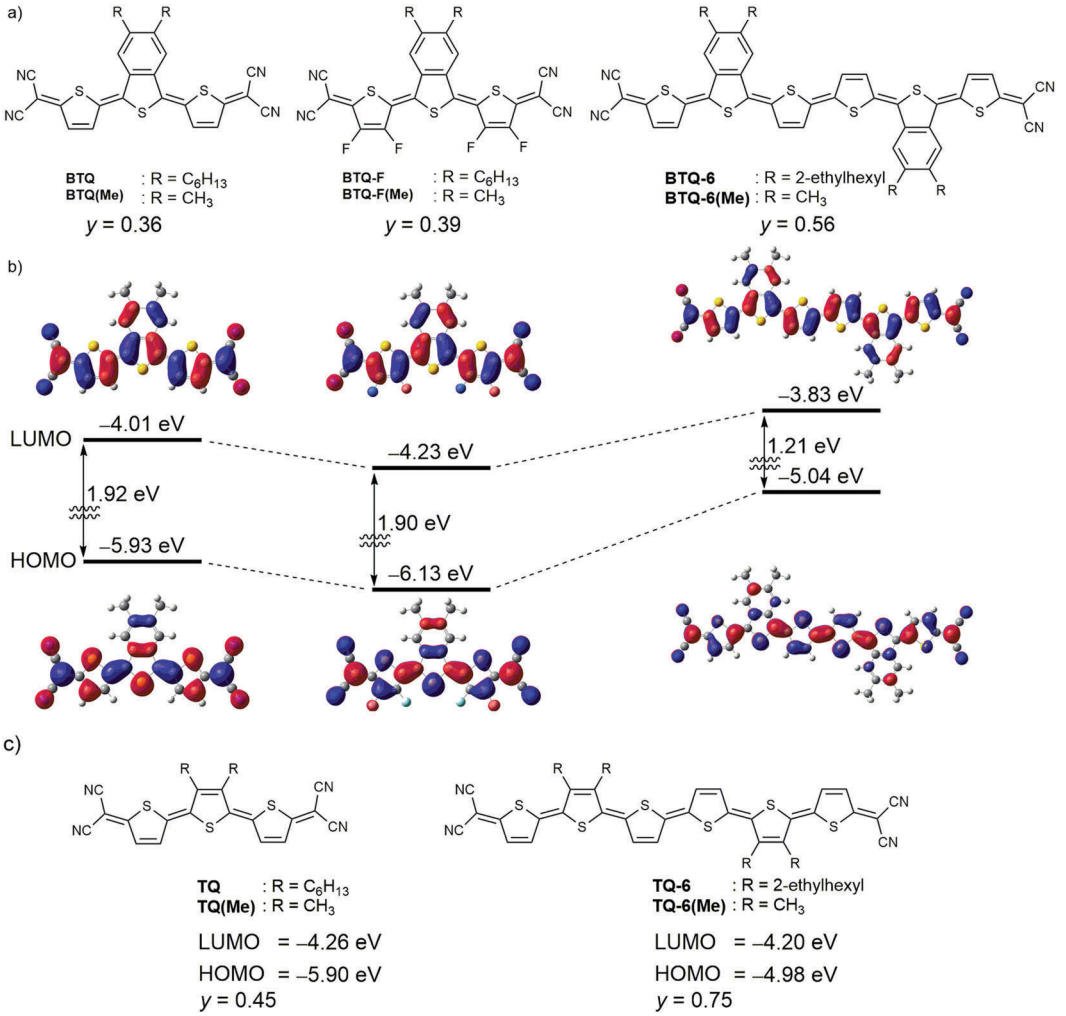


Fig. 1 (a) Chemical structures of compounds investigated in this study. (b) Calculated energy levels and orbitals for model compounds **BTQ(Me)** (left), **BTQ-F(Me)** (center), and **BTQ-6(Me)** (right). (c) Chemical structures of reference compounds.

compared to that of benzo[*c*]thiophene would allow us to create quinoidal oligothiophenes that have potential as air-stable semiconducting materials. To pursue this possibility, we designed new bis(dicyanomethylene)-substituted quinoidal oligothiophenes (**BTQ** and **BTQ-6**) containing 5,6-dialkylbenzo[*c*]thiophene units (Fig. 1). Furthermore, in order to increase the electron-accepting ability of **BTQ**, fluorine substituents were introduced at the *β*-position of the quinoidal terthiophene (**BTQ-F**). In this contribution, we report on the synthesis, properties, structures, and OFET characteristics of these compounds. Although the parent bis(dicyanomethylene)benzo[*c*]thiophene was synthesized and characterized by Cava *et al.* in 1993,[17] its π-extended derivative has not been reported so far.

## Results and discussion

### Theoretical studies

To estimate the molecular structure and frontier orbital energies, we performed density functional theory (DFT) calculations at the B3LYP/6-31G(d,p) level of theory. All alkyl groups were replaced with methyl groups for the ease of the calculation. Optimized geometries of **BTQ(Me)**, **BTQ-F(Me)**, and **BTQ-6(Me)** showed a planar conformation which indicates that the introduction of the benzene annelation in the central thiophene ring of terthiophene does not increase the distortion with respect to the dihedral angle (Fig. 1(b)). The lowest unoccupied molecular orbital (LUMO) energy level of **BTQ(Me)** is higher compared to that of **TQ(Me)** (Fig. 1(b) and (c)) but is still located at a low level of −4.01 eV. The substitution of hydrogen atoms in the thiophene rings with fluorine atoms for **BTQ-F(Me)** led to a further decrease of the LUMO energy level to −4.23 eV, while maintaining a similar highest occupied molecular orbital (HOMO)–LUMO energy gap. It should be mentioned that the LUMO of both compounds is delocalized over the entire π-conjugated backbone including the annelated benzene ring, which is favorable for the intermolecular overlap of LUMOs between neighboring molecules in the solid state.[16b] On the other hand, the extension of π-conjugation from **BTQ(Me)** to **BTQ-6(Me)** mainly contributes to an increase of the HOMO energy level from −5.93 eV to −5.04 eV. The singlet

 

biradical character ($y$) of these quinoidal compounds was calculated by the natural orbital occupation number of the lowest unoccupied natural orbital with spin-unrestricted calculations at the UHF/6-31G(d) level.[18] Compounds **BTQ(Me)** and **BTQ-F(Me)** gave $y$ values of 0.36 and 0.39, respectively. As we expected, these values were smaller than that of the reference **TQ(Me)** ($y$ = 0.45). Similarly, **BTQ-6(Me)** showed a lower $y$ value of 0.56 compared to **TQ-6(Me)** (0.75). These results indicate that the introduction of the benzo[*c*]thiophene unit is effective in increasing the contribution of the quinoidal electronic structure in the ground state.

## Synthesis and characterization

Since 5,6-dialkyl derivatives of benzo[*c*]thiophene are not easily accessed from commercially available compounds, we applied a new synthetic route, which relies on the construction of the benzo[*c*]thiophene core from tetrasubstituted benzene (Scheme 1). Methyl diester compound **1** was converted to 2-pyridinyl ester **2**, which then reacted with Grignard reagents, generated from 2-bromothiophene or 2-bromo-3,4-difluoro-5-trimethylsilylthiophene, to give key intermediates **3a** and **3b**. The treatment of **3a** and **3b** with Davy's reagent led to the formation of the benzo[*c*]thiophene core, and the obtained terthiophene derivatives were then treated with *N*-bromosuccinimide (NBS) to afford **4a** and **4b**. Finally, palladium-catalyzed coupling reactions of **4a** and **4b** with sodium dicyanomethanide followed by oxidation with 2,3-dichloro-5,6-dicyano-*p*-benzoquinone (DDQ) afforded **BTQ** and **BTQ-F** in 40% and 30% yield, respectively. The hexyl groups in the benzo[*c*]thiophene moiety ensured the good solubility of the molecules. The synthetic route to **BTQ-6** from **5** prepared similarly to **4** is also shown in Scheme 1. Note that the 2-ethylhexyl groups on the benzo[*c*]thiophene core are essential for ensuring appropriate solubility of the quinoidal thiophene 6-mer. On the other hand, we cannot obtain pure **TQ-6** due to low chemical stability. The chemical structures of **BTQ**, **BTQ-F**, and **BTQ-6** were fully characterized by NMR spectroscopy and MS. Detailed synthesis and characterization are summarized in the ESI.†

In the $^1$H NMR spectrum of **BTQ** at 25 °C, two sets of signals with an integration ratio of 10 : 1 were observed in the aromatic region (Fig. 2),[5] and all the two-set peaks were assigned to *anti–anti* and *anti–syn* isomers of the quinoidal terthiophene backbone, respectively, by nuclear Overhauser effect measurements (Fig. S1 in the ESI†). On the other hand, almost one singlet signal was observed for **BTQ-F**. In order to investigate the isomerization behavior of **BTQ**, **BTQ-F**, and **TQ**, variable temperature (VT)-NMR measurements were performed at 0, 25, and 50 °C. As shown in Fig. 2, the spectra of **BTQ** and **BTQ-F** showed little temperature dependence. Furthermore, the isomer ratio of **BTQ** is constant, irrespective of the temperature. On the other hand, although the spectrum of **TQ** showed two sets of signals at 0 °C similarly to that of **BTQ**, small peaks originating from the *anti–syn* isomer broadened at 25 °C and merged with the main peaks at 50 °C, implying the equilibrium between the two isomers probably *via* an aromatic biradical form. Similar *anti–syn* equilibrium was also reported on tetracyano bithiophene quinoid at 25 °C.[19] These results indicate that the quinoidal electronic structures of **BTQ** and **BTQ-F** are stabilized owing to the reduced contribution of the biradicaloid structure by benzene annulation. In addition, the presence of fluorine atoms on the thiophene rings in **BTQ-F** induces not only steric congestion in the *syn* form but also intramolecular S–F attractive interactions, forming fixed *anti* configurations between adjacent thiophene rings.[20] In contrast, **BTQ-6** showed broad signals even under a low temperature of −45 °C (Fig. S2, ESI†), indicating the presence of equilibrium between the isomers.

## Photophysical and electrochemical properties

The UV-vis-NIR absorption spectra of **BTQ**, **BTQ-F**, **BTQ-6**, and **TQ** in $CH_2Cl_2$ solutions are shown in Fig. 3, and the photophysical data are summarized in Table 1. The absorption spectra of **BTQ** and **BTQ-F** showed similar shapes with an absorption maximum ($\lambda_{max}$) at around 640 nm, which are slightly blue-shifted compared to that of **TQ** ($\lambda_{max}$ = 670 nm) (Fig. 3(a)). These intense bands are mainly assigned to the HOMO–LUMO transition by time-dependent (TD)-DFT calculations at the B3LYP/6-31G(d,p) level of theory (see the ESI†). The qualitative trend of molar extinction coefficients ($\varepsilon$) for these compounds is in good accordance with the estimated oscillator strength. As summarized in Table 1, the optical HOMO–LUMO energy gaps ($\Delta E_g^{opt}$) of these compounds estimated from the onsets in the absorption spectra

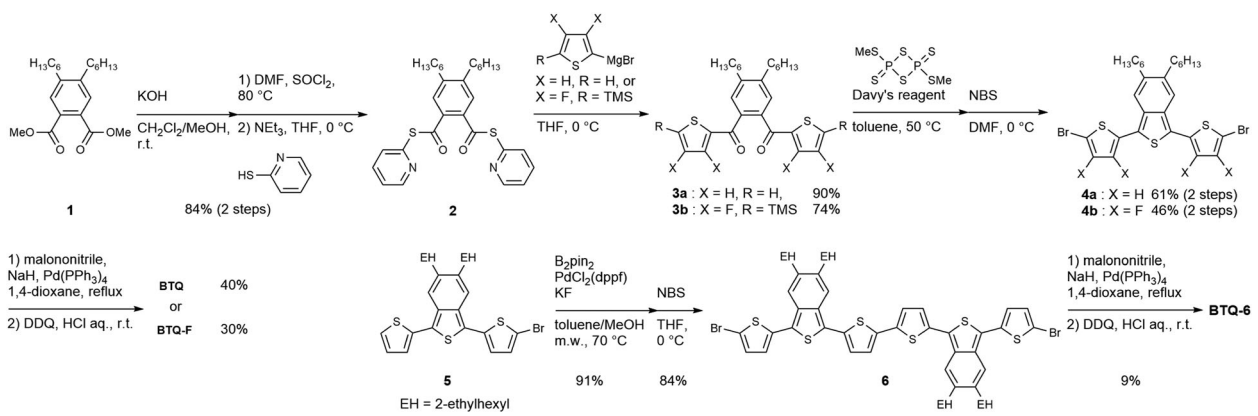


Scheme 1 Synthetic route to **BTQ**, **BTQ-F**, and **BTQ-6**.

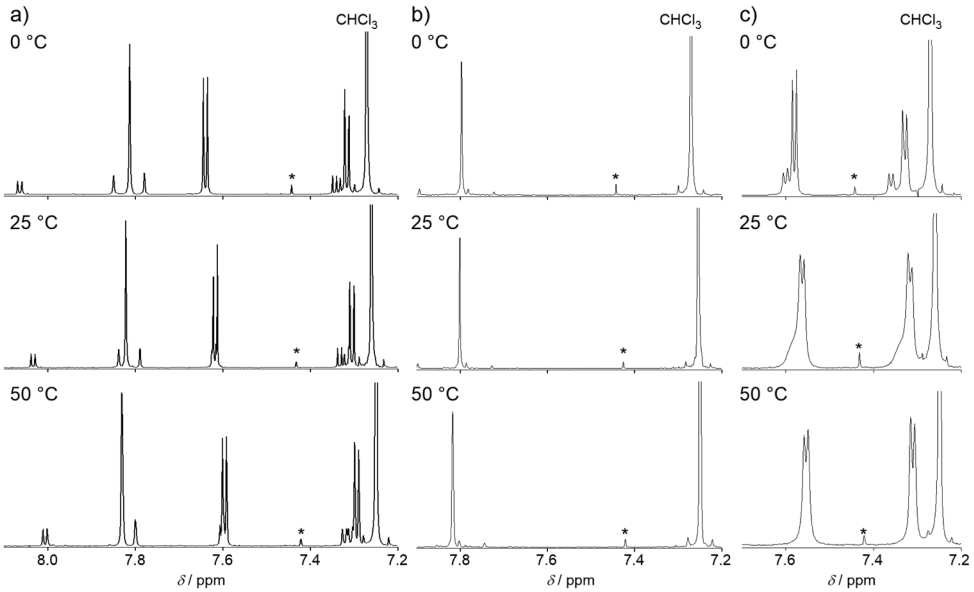


Fig. 2 VT-NMR spectra of (a) **BTQ**, (b) **BTQ-F**, and (c) **TQ** in the aromatic regions in $CDCl_3$. Signals marked by an asterisk are satellite peaks in $CHCl_3$.

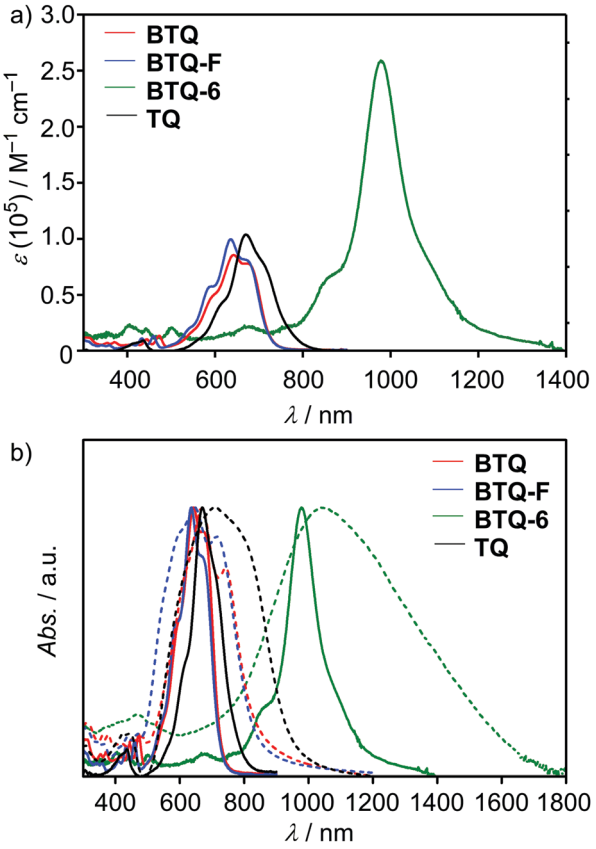


Fig. 3 (a) UV-vis-NIR absorption spectra of **BTQ** (red) and **BTQ-F** (blue), **TQ** (black), and **BTQ-6** (green) in $CH_2Cl_2$ and (b) in $CH_2Cl_2$ (solid line) and thin films (dashed line).

are found to be *ca.* 1.7 eV. The absorption spectrum of **BTQ-6** in $CH_2Cl_2$ solution exhibited an absorption band at the near-infrared region ($\lambda_{max}$ = 978 nm) with a large $\varepsilon$ of 2.6 × $10^5$ $M^{-1}$ $cm^{-1}$.

Table 1 Photophysical and electrochemical properties

| Compound | $\lambda_{max}$[a] ($\varepsilon$ × $10^5$)/ nm ($M^{-1}$ $cm^{-1}$) | $\Delta E_g^{opt}$[a]/ eV | $E_{1/2}^{ox}$[b]/ V | $E_{1/2}^{red}$[b]/ V | $E_{HOMO}$[c]/ eV | $E_{LUMO}$[d]/ eV |
|---|---|---|---|---|---|---|
| **BTQ** | 642 (0.9) | 1.70 | 0.86 | −0.74 | −5.66 | −4.06 |
| **BTQ-F** | 636 (1.0) | 1.71 | 1.05 | −0.50 | −5.85 | −4.30 |
| **BTQ-6** | 978 (2.6) | 1.14 | 0.08 | −0.54 | −4.88 | −4.26 |
| | | | 0.35 | −0.61 | | |
| **TQ** | 670 (1.1) | 1.60 | 0.81 | −0.58 | −5.61 | −4.23 |

[a] In $CH_2Cl_2$. [b] In $CH_2Cl_2$ containing 0.1 M $TBAPF_6$. V *vs.* $Fc/Fc^+$. [c] $E_{HOMO} = -E_{1/2}^{ox} - 4.8$. [d] $E_{LUMO} = -E_{1/2}^{red} - 4.8$.

This behavior is in contrast to a previous report where quinoidal sexithiophene showed a reduced molar extinction coefficient with concomitant appearance of marked absorptions in the visible region, compared to the corresponding quinoidal quinquethiophene. The reduced extinction coefficient was attributed to the high contribution of the biradical character,[14b] which indicates that the high $\varepsilon$ of **BTQ-6** is rationalized by the higher contribution of the quinoidal electronic structure owing to the presence of benzo[*c*]thiophene units in the framework. Compared to the solution spectra, well-structured shoulders with red-shifted $\lambda_{max}$ were observed for **BTQ** and **BTQ-F** in thin films (Fig. 3(b)). This phenomenon is attributed to the intermolecular electronic interactions of π−π stacked backbones, which are favorable for carrier transport in thin-film devices. The absorption spectrum of **BTQ-6** in thin films showed a broad absorption with the onset reaching 1800 nm. Such a large bathochromic shift was observed for quinoidal quaterthiophene.[9] In addition to the intermolecular electronic interactions, the existence of the biradical character may have influence on this bathochromic shift.

The electrochemical properties of these compounds were investigated by cyclic voltammetry (CV) measurements in $CH_2Cl_2$ containing 0.1 M tetrabutylammonium hexafluorophosphate ($TBAPF_6$) as the supporting electrolyte. All potentials are

 

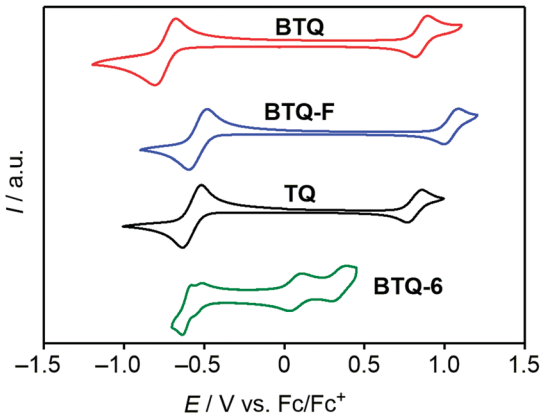


Fig. 4 Cyclic voltammograms of **BTQ** (red) and **BTQ-F** (blue), **TQ** (black), and **BTQ-6** (green) in $CH_2Cl_2$ containing 0.1 M $TBAPF_6$.

calibrated against a ferrocene/ferrocenium ($Fc/Fc^+$) couple as the standard, and these values are listed in Table 1. As presented in Fig. 4, the cyclic voltammograms of **BTQ**, **BTQ-F**, and **TQ** showed one reversible oxidation wave and a reduction wave. The observed good reversibility indicates the stable formation of both cationic and anionic species. Integration of each peak area for these compounds implied the participation of one electron and two electrons in oxidation and reduction processes, respectively. As shown in Table 1, due to the electron-withdrawing nature of fluorine atoms, both the half-wave oxidation potential ($E^{ox}_{1/2}$) and reduction potential ($E^{red}_{1/2}$) of **BTQ-F** are positively shifted compared to those of **BTQ**. Based on the assumption that the energy level of $Fc/Fc^+$ is −4.8 eV below the vacuum level,[21–23] the LUMO energy levels ($E_{LUMO}$) of **BTQ** and **BTQ-F** were estimated to be −4.06 and −4.30 eV, respectively. These values are in good agreement with those estimated from the theoretical calculation. For **BTQ-6**, two reversible oxidation and reduction processes were observed. The $E_{LUMO}$ and $E_{HOMO}$ of **BTQ-6** estimated from the first $E^{red}_{1/2}$ and $E^{ox}_{1/2}$ were −4.26 and −4.88 eV, respectively, indicating that the extension of the quinoidal π-system leads to a significant increase of the HOMO energy level. This qualitative trend of HOMO and LUMO energy levels is also in good agreement with the theoretical estimation.

### X-Ray single-crystal structures

The structure of **BTQ-F** was unambiguously determined using X-ray crystallographic analysis of the crystals that were grown by slow evaporation from a solution in ethyl acetate (EtOAc) and a MeOH mixed solvent. As shown in Fig. 5(a), the molecular structure of **BTQ-F** adopts all *anti* and planar conformations with dihedral angles of less than 2.7°. On the other hand, the distance of the intramolecular S–F contact (2.75 Å) is smaller than the sum of van der Waals radii of S and F atoms (3.27 Å), indicating the presence of nonbonding attractive interactions between these atoms. In the packing diagram, **BTQ-F** molecules are oriented in a face-to-face fashion with minimum intermolecular π–π distances of 3.55 Å and 3.42 Å (a and b in Fig. 5(b), respectively). On the basis of the calculation by the Amsterdam Density Functional program at the PW91/TZP level, the transfer

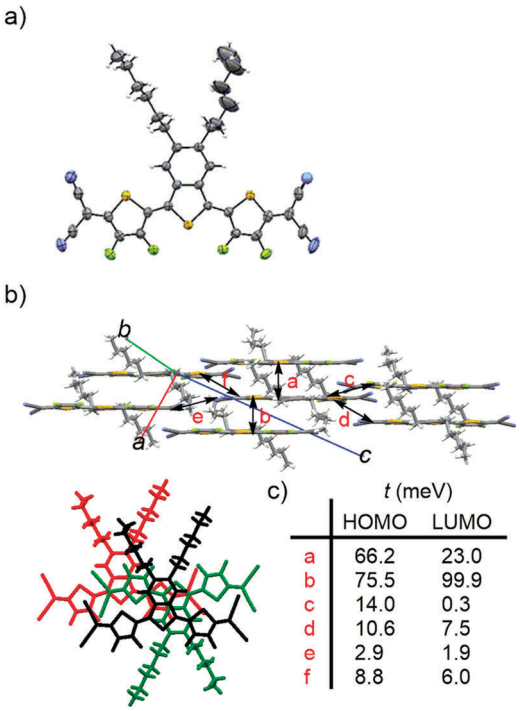


Fig. 5 (a) ORTEP drawing of the molecular structure, (b) packing diagram from side view (top) and top view (bottom), and (c) estimated transfer integrals of HOMOs and LUMOs for **BTQ-F**.

integrals between facial stacked structures of **BTQ-F** in the crystal were estimated. All the transfer integrals for electron transport ($t_{LUMO}$) and hole transport ($t_{HOMO}$) are shown in Fig. 5(c). **BTQ-F** showed a large $t_{HOMO}$ and $t_{LUMO}$ of 75.5 and 99.9 meV, respectively, which is expected to construct a charge-carrier transporting pathway along the stacking direction.

### Charge carrier transport and film morphologies

To evaluate the semiconducting charge-transport characteristics of **BTQ**, **BTQ-F**, **BTQ-6**, and **TQ**, OFET devices based on thin films were fabricated. Although there have been several reports on high or finely tuned ambipolar OFETs of ter- and quaterthiophene quinoids,[5] the compounds used in this work were characterized using a conventional bottom-gate bottom-contact transistor configuration with similar fabrication conditions for all devices. The active layer was prepared by spin-coating from a 0.3 wt% $CHCl_3$ solution onto hexamethyldisilazane (HMDS)-modified $Si/SiO_2$ substrates. Thermal annealing was effective for improving the performance for **BTQ** and **BTQ-F**, and the current–voltage characteristics of best-performance devices are shown in Fig. 6 and Fig. S3, S4 (ESI†). The hole ($\mu_h$) and electron mobilities ($\mu_e$) were extracted from the transfer characteristics at constant source–drain voltages. The corresponding device parameters such as mobility, threshold voltage ($V_{th}$), and current on/off ratio ($I_{on}/I_{off}$) are summarized in Table 2. Both **BTQ** and **BTQ-F** revealed solely an electron transport with $\mu_e$ in the order of $10^{-3}$ $cm^2$ $V^{-1}$ $s^{-1}$ due to their low-lying LUMO energy levels. Furthermore, OFETs based on these compounds retained the same order of $\mu_e$ under air-exposed conditions. While the **TQ**-based device exhibited a higher

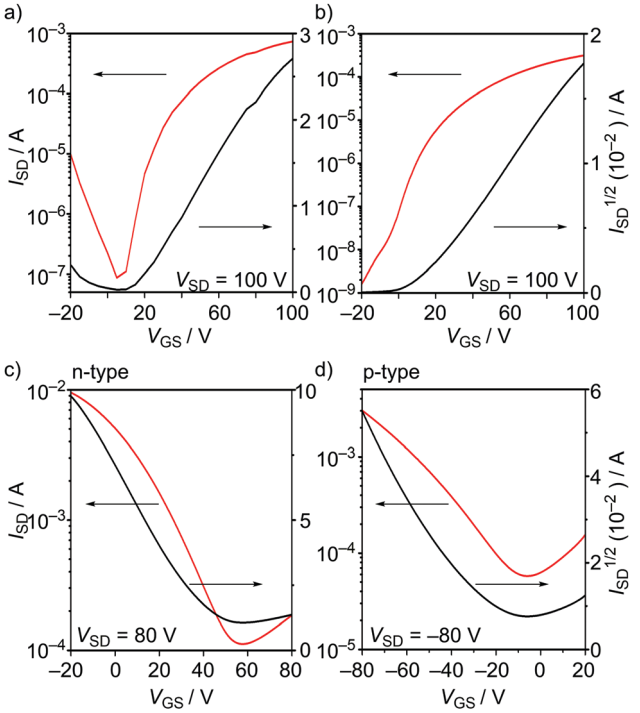


Fig. 6 (a) Transfer characteristics of OFETs using (a) **BTQ**, (b) **BTQ-F**, (c) **BTQ-6**, and (d) **BTQ-6**. $V_{GS}$, $I_{SD}$, and $V_{SD}$ denotes gate voltage, source–drain current, and source–drain voltage, respectively.

Table 2 Field-effect characteristics under vacuum and in air

| Compounds | Anneal temp./°C | $V_{th}$/V | $I_{on}/I_{off}$ | $\mu_e$/cm$^2$ V$^{-1}$ s$^{-1}$ ($\mu_h$/cm$^2$ V$^{-1}$ s$^{-1}$) |
|---|---|---|---|---|
| **BTQ**[a] | 170 | 15 | $10^4$ | $3.4 \times 10^{-3}$ |
| **BTQ**[b] | 170 | 18 | $10^5$ | $2.5 \times 10^{-3}$ |
| **BTQ-F**[a] | 170 | 13 | $10^5$ | $1.2 \times 10^{-3}$ |
| **BTQ-F**[b] | 170 | −9.4 | $10^3$ | $3.0 \times 10^{-4}$ |
| **TQ**[a] | As cast | 35 | $10^1$ | $3.3 \times 10^{-2}$ |
| **TQ**[b] | 150 | 22 | $10^2$ | $3.4 \times 10^{-2}$ |
| **BTQ-6** | As cast | 78 | $10^1$ | $8.9 \times 10^{-4}$ |
| | (As cast)[c] | (−29)[c] | ($10^2$)[c] | ($3.1 \times 10^{-2}$)[c] |

[a] Under vacuum. [b] In air. [c] Hole-transporting characteristics are shown in parenthesis.

$\mu_e$ compared with **BTQ** and **BTQ-F**, the $I_{on}/I_{off}$ ratio was quite low due to a high off source–drain current (Fig. S4(d), ESI†). This might indicate that the ambipolar character of the **TQ** framework affects the increase of carrier density even in the off state.[6b]

In order to investigate the film properties of these compounds, X-ray diffraction (XRD) and atomic force microscopy (AFM) measurements of these thin films on HMDS-modified Si/$SiO_2$ substrates were performed. As shown in Fig. 7 and Fig. S5 (ESI†), these compounds exhibited clear diffraction peaks in X-ray diffractogram (XRD), indicating the formation of crystalline structures in thin films. The peak of **BTQ-F** at $2\theta = 6.2°$ can be indexed as the (011) diffraction peak with a $d$ spacing of 14.2 Å according to the above-mentioned X-ray crystal structure analysis. Thus, the **BTQ-F** molecules are edge-on arranged with the stacking direction parallel to the $SiO_2$ surface. While the AFM image of **BTQ** revealed crystal-shaped

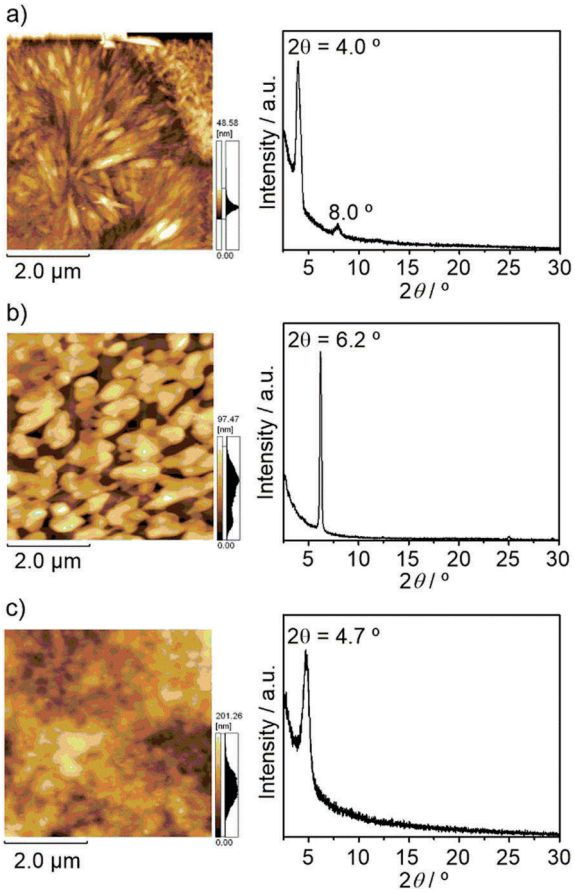


Fig. 7 AFM height images and XRD data of (a) **BTQ**, (b) **BTQ-F**, and (c) **BTQ-6**.

micrometer-sized grains, **BTQ-F** showed a rough film surface with large crystal grains (Fig. 7). Both **BTQ** and **BTQ-F** maintained OFET responses under air-exposed conditions, irrespective of the difference of the film morphologies. This result indicates that the observed air-stability mainly originates from the thermodynamic stability, *i.e.*, a low LUMO energy level of less than −4.0 eV. As discussed above, the introduction of benzene annelation led to the isomerization behavior different from that of **TQ** against temperature change. Therefore, to investigate the influence of the benzene annelation on the device characteristics, temperature-dependent OFET measurements of **BTQ**- and **TQ**-based devices were performed. For these measurements, we performed the surface modification of the source and drain gold electrodes using hexadecanethiol to minimize the contact resistance between Au electrodes and active layer.[24] The decreased contact resistance was confirmed by the output characteristics (Fig. S6, ESI†).

As shown in Fig. 8(a), OFETs using **BTQ** showed a decrease of electron mobility with decreasing temperature. This phenomenon is in agreement with the temperature dependence of hopping dominated carrier transport.[25] The activation energy of **BTQ** was estimated to be 0.13 eV (Fig. S7, ESI†). On the other hand, the **TQ**-based device showed a reverse trend with a decrease in the off current (Fig. 8(b)). We speculate that the diminution of the biradical character for **BTQ** might facilitate the inherent

 

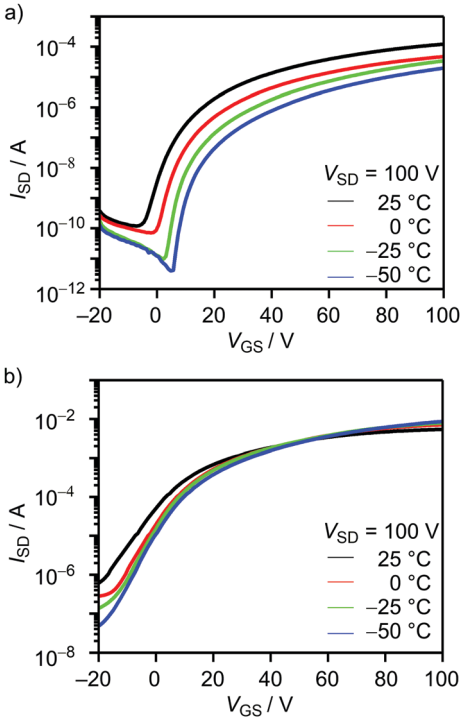


Fig. 8 Temperature-dependent transfer characteristics of the 1-hexadecanethiol-treated OFETs using (a) **BTQ** and (b) **TQ**.

electron transport, which means that biradicals act as carriers. Although the presence of the sterically bulky 2-ethylhexyl groups may prevent dense π–π stacking, XRD results indicate the crystalline structures in thin films (Fig. 7(c)). In fact, OFET devices based on **BTQ-6** showed not only electron-transporting characteristics ($8.9 \times 10^{-4}$ cm$^2$ V$^{-1}$ s$^{-1}$) but also hole-transporting characteristics ($3.1 \times 10^{-2}$ cm$^2$ V$^{-1}$ s$^{-1}$). The appearance of p-type behavior can be explained by the increased HOMO energy levels. Note that the field-effect response for the quinoidal thiophene 6-mer is not reported so far. The OFET devices based on **BTQ**, **TQ**, and **BTQ-6** were stored and measured periodically under the air-exposed conditions. As shown in Fig. S8 (ESI†), compared to **TQ**, a decrease of carrier mobility is suppressed for benzo[*c*]thiophene-containing semiconductors. We have considered that the introduction of the benzene annelation to form a stabilized quinoidal electronic structure becomes an effective strategy in developing new semiconducting materials.

## Conclusions

In summary, to investigate the influence of benzene-annelation on the stabilization of the quinoidal electronic structure, we successfully synthesized new bis(dicyanomethylene)-substituted quinoidal oligothiophenes containing benzo[*c*]thiophene units. We also developed quinoidal oligothiophenes containing both a benzo[*c*]thiophene unit and fluorinated thiophenes. Theoretical calculations as well as experimental results indicate that the introduction of benzo[*c*]thiophene into the oligothiophene π-conjugated quinoid system is effective in stabilizing quinoidal electronic structures. These molecules showed good electron-transporting characteristics, and the extension of π-conjugation from thiophene 3-mer to 6-mer led to the appearance of both hole- and electron-transporting characteristics. These results show that quinoidal π-conjugated systems containing benzo[*c*]thiophene units show potential as candidates for semiconducting materials using stabilized quinoidal structures. Further investigations toward expansion of the π-conjugation are currently underway in our group.

## Conflicts of interest

There are no conflicts to declare.

## Acknowledgements

This work was supported by a Grant-in-Aid for Scientific Research (B) (16H04191) and Innovative Areas (JP25110004) and ''Dynamic Alliance for Open Innovation Bridging Human, Environmental and Materials'' from the Ministry of Education, Culture, Sports, Science and Technology, Japan, and ACT-C programs from the Japan Science and Technology Agency Japan. Thanks are extended to the Comprehensive Analysis Center (CAC), ISIR, for assistance in elemental analysis and HRMS. Open Access funding provided by the Max Planck Society.

## Notes and references

1 (*a*) A. Mishra, C.-Q. Ma and P. Bäuerle, *Chem. Rev.*, 2009, **109**, 1141–1276; (*b*) K. Takimiya, S. Shinamura, I. Osaka and E. Miyazaki, *Adv. Mater.*, 2011, **23**, 4347–4370; (*c*) Y. Zhao, Y. Guo and Y. Liu, *Adv. Mater.*, 2013, **25**, 5372–5391; (*d*) J. Roncali, P. Leriche and P. Blanchard, *Adv. Mater.*, 2014, **26**, 3821–3838; (*e*) S. M. McAfee, J. M. Topple, I. G. Hill and G. C. Welch, *J. Mater. Chem. A*, 2015, **3**, 16393–16408.
2 (*a*) J. Yang, D. Yan and S. T. Jones, *Chem. Rev.*, 2015, **115**, 5570–5603; (*b*) O. Ostroverkhova, *Chem. Rev.*, 2016, **116**, 13279–13412.
3 K. Deuchert and S. Hünig, *Angew. Chem., Int. Ed.*, 1978, **17**, 875–886.
4 (*a*) J. B. Torrance, *Acc. Chem. Res.*, 1979, **12**, 79–86; (*b*) N. Martín, J. L. Segura and C. Seoane, *J. Mater. Chem.*, 1997, **7**, 1661–1676.
5 J. Casado, R. P. Ortiz and J. T. L. Navarrete, *Chem. Soc. Rev.*, 2012, **41**, 5672–5686.
6 (*a*) T. M. Pappenfus, R. J. Chesterfield, C. D. Frisbie, K. R. Mann, J. Casado, J. D. Raff and L. L. Miller, *J. Am. Chem. Soc.*, 2002, **124**, 4184–4185; (*b*) R. J. Chesterfield, C. R. Newman, T. M. Pappenfus, P. C. Ewbank, M. H. Haukaas, K. R. Mann, L. L. Miller and C. D. Frisbie, *Adv. Mater.*, 2003, **15**, 1278–1282; (*c*) D. E. Janzen, M. W. Burand, P. C. Ewbank, T. M. Pappenfus, H. Higuchi, D. A. da Silva Filho, V. G. Young, J.-L. Brédas and K. R. Mann, *J. Am. Chem. Soc.*, 2004, **126**, 15295–15308.
7 S. Handa, E. Miyazaki, K. Takimiya and Y. Kunugi, *J. Am. Chem. Soc.*, 2007, **129**, 11684–11685.

8 (*a*) J. C. Ribierre, T. Fujihara, S. Watanabe, M. Matsumoto, T. Muto, A. Nakao and T. Aoyama, *Adv. Mater.*, 2010, **22**, 1722–1726; (*b*) J.-C. Ribierre, S. Watanabe, M. Matsumoto, T. Muto, A. Nakao and T. Aoyama, *Adv. Mater.*, 2010, **22**, 4044–4048; (*c*) J. C. Ribierre, S. Watanabe, M. Matsumoto, T. Muto and T. Aoyama, *Appl. Phys. Lett.*, 2010, **96**, 083303.

9 J. Li, X. Qiao, Y. Xiong, W. Hong, X. Gao and H. Li, *J. Mater. Chem. C*, 2013, **1**, 5128–5132.

10 (*a*) Y. Qiao, Y. Guo, C. Yu, F. Zhang, W. Xu, Y. Liu and D. Zhu, *J. Am. Chem. Soc.*, 2012, **134**, 4084–4087; (*b*) Y. Qiao, J. Zhang, W. Xu and D. Zhu, *J. Mater. Chem.*, 2012, **22**, 5706–5714; (*c*) Q. Wu, S. Ren, M. Wang, X. Qiao, H. Li, X. Gao, X. Yang and D. Zhu, *Adv. Mater.*, 2013, **23**, 2277–2284.

11 Y. Xiong, J. Tao, R. Wang, X. Qiao, X. Yang, D. Wang, H. Wu and H. Li, *Adv. Mater.*, 2016, **28**, 5949–5953.

12 (*a*) Q. Wu, R. Li, W. Hong, H. Li, X. Gao and D. Zhu, *Chem. Mater.*, 2011, **23**, 3138–3140; (*b*) Q. Wu, S. Ren, M. Wang, X. Qiao, H. Li, X. Gao, X. Yang and D. Zhu, *Adv. Funct. Mater.*, 2013, **23**, 2277–2284; (*c*) J. Li, X. Qiao, Y. Xiong, H. Li and D. Zhu, *Chem. Mater.*, 2014, **26**, 5782–5788.

13 T. Mori, N. Yanai, I. Osaka and K. Takimiya, *Org. Lett.*, 2014, **16**, 1334–1337.

14 (*a*) V. Hernández, S. C. Losada, J. Casado, H. Higuchi and J. T. L. Navarrete, *J. Phys. Chem. A*, 2000, **104**, 661–672; (*b*) T. Takahashi, K.-i. Matsuoka, K. Takimiya, T. Otsubo and Y. Aso, *J. Am. Chem. Soc.*, 2005, **127**, 8928–8929; (*c*) R. P. Ortiz, J. Casado, V. Hernández, J. T. L. Navarrete, P. M. Viruela, E. Ortí, K. Takimiya and T. Otsubo, *Angew. Chem., Int. Ed.*, 2007, **46**, 9057–9061; (*d*) E. V. Canesi, D. Fazzi, L. Colella, C. Bertarelli and C. Castiglioni, *J. Am. Chem. Soc.*, 2012, **134**, 19070–19083; (*e*) R. Kishi, M. Dennis, K. Fukuda, Y. Murata, K. Morita, H. Uenaka and M. Nakano, *J. Phys. Chem. C*, 2013, **117**, 21498–21508; (*f*) L. Colella, L. Brambilla, V. Nardone, E. Parisini, C. Castiglioni and C. Bertarelli, *Phys. Chem. Chem. Phys.*, 2015, **17**, 10426–10437; (*g*) S. Ray, S. Sharma, U. Salzner and S. Patil, *J. Phys. Chem. C*, 2017, **121**, 16088–16097.

15 F. Wudl, M. Kobayashi and A. J. Heeger, *J. Org. Chem.*, 1984, **49**, 3382–3384.

16 (*a*) C. Zhang, Y. Zang, E. Gann, C. R. McNeill, X. Zhu, C.-a. Di and D. Zhu, *J. Am. Chem. Soc.*, 2014, **136**, 16176–16184; (*b*) C. Zhang, Y. Zang, F. Zhang, Y. Diao, C. R. McNeill, C.-a. Di, X. Zhu and D. Zhu, *Adv. Mater.*, 2016, **28**, 8456–8462; (*c*) L. Ren, H. Fan, D. Huang, D. Yuan, C.-a. Di and X. Zhu, *Chem. – Eur. J.*, 2016, **22**, 17136–17140; (*d*) L. Ren, D. Yuan, E. Gann, Y. Guo, L. Thomsen, C. R. McNeill, C.-a. Di, Y. Yi, X. Zhu and D. Zhu, *Chem. Mater.*, 2017, **29**, 4999–5008; (*e*) C. Zhang, D. Yuan, H. Wu, E. Gann, L. Thomsen, C. R. McNeill, C.-a. Di, X. Zhu and D. Zhu, *J. Mater. Chem. C*, 2017, **5**, 1935–1943.

17 D. Lorcy, K. D. Robinson, Y. Okuda, J. L. Atwood and M. P. Cava, *J. Chem. Soc., Chem. Commun.*, 1993, 345–347.

18 R. Kishi, S. Ochi, S. Izumi, A. Makino, T. Nagami, J.-y. Fujiyoshi, N. Matsushita, M. Saito and M. Nakano, *Chem. – Eur. J.*, 2016, **22**, 1493–1500.

19 H. Higuchi, S. Yoshida, Y. Uraki and J. Ojima, *Bull. Chem. Soc. Jpn.*, 1998, **71**, 2229–2237.

20 P. Metrangolo, H. Neukirch, T. Pilati and G. Resnati, *Acc. Chem. Res.*, 2005, **38**, 386–395.

21 A. J. Bard and L. R. Faulkner, *Electrochemical Methods-Fundamentals and Applications*, Wiley, New York, 1984.

22 J. Pommerehne, H. Vestweber, W. Guss, R. F. Mahrt, H. Bassler, M. Porsch and J. Daub, *Adv. Mater.*, 1995, **7**, 551–554.

23 C. M. Cardona, W. Li, A. E. Kaifer, D. Stockdale and G. C. Bazan, *Adv. Mater.*, 2011, **23**, 2367–2371.

24 K. Asadi, F. Gholamrezaie, E. C. P. Smits, P. W. M. Blom and B. de Boer, *J. Mater. Chem.*, 2007, **17**, 1947–1953.

25 A. Pivrikas, M. Ullah, H. Sitter and N. S. Sariciftci, *Appl. Phys. Lett.*, 2011, **98**, 092114.